www.sciencemag.org/cgi/content/full/311/5761/660/DC1

Supporting Online Material for

Fish Population and Behavior Revealed by Instantaneous Continental Shelf–Scale Imaging

Nicholas C. Makris,* Purnima Ratilal, Deanelle T. Symonds, Srinivasan Jagannathan, Sunwoong Lee, Redwood W. Nero

*To whom correspondence should be addressed. E-mail: makris@mit.edu

Published 3 February 2006, *Science* **311**, 660 (2006)
DOI: 10.1126/science.1121756

This PDF file includes:

Other Supporting Online Material for this manuscript includes the following:
(available at www.sciencemag.org/cgi/content/full/311/5761/660/DC1)

Materials and Methods

Our field measurements show that the areal density, dynamics, and behavior of fish populations can be continuously monitored with minute-to-minute updates over thousands of square kilometers by the use of ocean-acoustic waveguide remote sensing (OAWRS) in continental shelf-environments.

Movie S1 shows the detailed time-space behavior of fish groups in and around the large shoal during daylight hours on 14 May 2003. Frames are updated every 50 s. From 11:31:35 EDT to 12:47:25 EDT, a conventional fish finding sonar (CFFS) track is overlain including the transect illustrated in Fig. 2, A to E. A moving circle, indicating the position of the CFFS measurement, turns black when CFFS fish group density is greater than V_{shoal} and white when it is less than V_{shoal}. Co-registration of dense fish groups between the two systems is found to be high. The movie illustrates the continuous evolution of shoal morphology, from consolidation in the morning to fragmentation in the afternoon, also shown by the series of snapshots in Fig. 3, A to E. The shoal often evolves into an hourglass pattern and occasionally splits in two and rejoins before fragmentation. Small isolated fish groups are observed moving throughout the area during the day.

A waveguide is a bounded medium that efficiently channels propagating waves (*S1*). In free space, the intensity (power per unit area) of waves propagating from a point source to a distant receiver is inversely proportional to the square of the range from the source to the receiver. Source power is geometrically spread over spherical areas that increase with the square of this range. In a waveguide, spreading loss is determined by the geometry of the bounded medium. In a one-dimensional tube of constant cross-section, source power no longer spreads as range increases beyond the tube diameter, so that the mean sound intensity over the cross-section stays fixed. As a medium for acoustic waves, the ocean is bounded by the air above and the seafloor below. For ranges much greater than the ocean depth, where OAWRS is particularly useful, loss in mean intensity due to geometric spreading occurs over cylindrical areas, increasing in direct proportion to range if ocean depth is constant or nearly constant, as it typically is. Conventional fish finding sonar (CFFS) operates over ranges less than or on the order of the local ocean depth, and so is typically governed by the spherical spreading loss encountered in free-space. OAWRS also uses lower frequency waves that suffer far less attenuation from absorption and scattering (*S2*-*S5*) in the medium than the waves used by CFFS (*S6, S7*).

We have generated wide-area movies detailing the spatial-temporal dynamics of fish group behavior by concatenating sequences of OAWRS images. If the temporal sampling rate is too slow, slower than twice the rate of non-negligible spatial-temporal change (the Nyquist rate (*S8*)), a movie would appear to be aliased (*S8*) in time. This means that it would not be possible to determine all the important continuous motion over time in a scene. When aliasing occurs, motions at frequencies higher than the sampling rate become confused with low frequency motions. Examples of temporal aliasing include the discontinuous motion in viewing old movies with low frame rates, people moving in a dark room lit only by an infrequently flashing strobe light, and the illusion of slow backward or forward rotation on the spokes of a rapidly moving bicycle wheel. Similarly, sampling a spatial scene too sparsely, below the spatial Nyquist rate, leads to an inability to reconstruct its continuous spatial dependence. Our movies show no apparent signs of

spatial or temporal aliasing. This follows from spectral analysis, where, for example, the spectrum of total fish population follows a consistent decaying power law all the way to the highest frequencies (Fig. S1-B), and shows an autocorrelation time scale (Fig. S1-A) much larger than the sampling interval between OARS snapshots. The lack of aliasing follows from the fact that each wide-area OAWRS image also represents an effectively instantaneous scene (*S9*-*S11*), since the total measurement duration is shorter than the time-scale of resolvable spatial change across the scene. It takes a fish longer to swim across one of our 30-m range resolution cells (at a speed typically less than 1 m/s) than for the acoustic wave (traveling at roughly 1500 m/s) to interact with all scatterers in one of our wide area OAWRS images (roughly 30 km radius). Our overall scenes are effectively instantaneous even in the presence of fish density waves since these were highly localized in our survey area, spanning scales less than 3 km, and travel at least two orders of magnitude slower than the speed of acoustic waves (Fig. S1-C).

To form an instantaneous OAWRS image, a vertical source array sends a short broadband transmission of sound out omni-directionally in horizontal azimuth. As they travel, the sound waves reflect from the sea surface and bottom to form standing waves in depth that are called waveguide modes. These are analogous to the normal modes of a vibrating guitar string, where the entire vertical water column of the ocean acts like the plucked string. As the modes propagate horizontally outward from the source, they interact with and scatter from environmental features along the way. Scattered returns from environmental features are then continuously received by a horizontally towed line array and charted in horizontal range and bearing by temporal matched filtering and planewave beamforming (*S2, S4, S12*). The resulting image is an instantaneous snapshot of the ocean waveguide environment over the two-way travel times of the signal returns. OAWRS range resolution is fixed at the mean sound speed, c = 1475 m/s, divided by twice the signal bandwidth, or roughly 15 m before averaging. Theory, modeling, and our field measurements using calibrated targets with known positions show that ranging error of OAWRS is negligible since it is on the order of the 30 m range resolution of our image pixels after averaging, and as a consequence of modal propagation, is insensitive to the depth of scatterers or environmental features in the waveguide. OAWRS azimuthal resolution in radians varies as the acoustic wavelength λ divided by the projected array length $L\cos\theta$, where L is the full array length and the azimuth angle θ is zero at *broadside*, which is normal to the array axis. At *endfire*, parallel to the array axis, the resolution becomes roughly $\sqrt{2\lambda / L}$ radians. A sketch of our source array appears in Fig. 5 of Ref. (*S4*). Our receiving array is similar to that shown in the same figure except that it was comprised of 64-elements over a total aperture of 94.5 m. A top-down view of the bistatic measurement geometry, including the varying spatial resolution footprint of the sonar, appears in Fig. A1 of Ref. (*S13*). The beamwidth of the CFFS used in our field experiment (Fig. 2E) is 6.8°, which yields a circular 70 m^2 areal resolution footprint at 80-m depth where many of the fish groups we imaged were concentrated.

In OAWRS, the entire water column is insonified by the up-and-down going planewave components forming each waveguide mode. During our 2003 OAWRS experiment, measurements of the mean acoustic intensity after one-way transmission from the source to receiver, as well as two-way returns from the seafloor, show no sign of modal interference structure, such as peaks and nulls from coherent interference. Rather a uniform decay with range is observed, indicating a lack of modal interference, which

corresponds to a highly predictable and uniformly mixed acoustic structure over depth. This is expected for a number of reasons. Environmental scatterers such as seafloor inhomogeneities and fish are distributed randomly within the sonar resolution footprint and so decorrelate modes in the acoustic field (*S4, S14*), which then obeys circular complex Gaussian Random field (CCGRF) statistics (*S2, S9-S11, S15*), by the central limit theorem. The intensity of a CCGRF is characterized by signal-dependent noise known as speckle noise (*S9-S11*). The ocean is also active, with internal waves, eddies and turbulence. These cause small sound-speed changes in time and space that typically cause acoustic modes to decorrelate, which again leads to CCGRF fluctuations at the receiver by the central limit theorem (*S11, S15*). The one-way acoustic field measurements during our 2003 OAWRS experiment followed CCGRF statistics over time, which is consistent with the observed lack of modal interference structure in range. These observations and the consequential lack of modal interference structure in depth were verified by simulations where sound speed variations measured during our experiment were input to statistical models for waveguide propagation in the continental shelf (*S16, S17*). (Even without randomness in the medium, broadband transmissions, such as ours, also lack the delicate modal-interference nulls found in deterministic single-frequency transmission.) As a consequence of acoustic tunneling, OAWRS insonification in the upper sediment is similar to that in the water so there is no sharp boundary in the acoustic field at the water-sediment interface. In our 2003 experiment, fish shoals observed with CFFS were always found in the lower half of the watercolum, typically in layers roughly 10-m thick within meters of the seafloor, even during the dramatic population changes shown in Fig 3.

CFFS typically operates in the 20-500kHz range and measures the local depth distribution of fish at any instant by echo sounding within a narrow downward-directed beam along the line transect of a slowly moving research vessel (*S18-S21*). CFFS surveys habitats at rates in the vicinity of 0.2 km^2/hour, which are similar to those of capture-trawl vessels. Survey rates can increase by roughly an order of magnitude when standard multi-beam or side-scan technology, which also exploits local, linear, waterborne propagation paths, is used to augment CFFS (*S20, S22*). CFFS methods have provided evidence for structural similarity and been used to describe dynamic behavior in fish groups over small scales, tens to hundreds of meters (*S22-S29*). Previously, the closest to a true snapshot of the horizontal morphology and spatial distribution of a typical large shoal, of roughly 10 km length, was generated by a synthetic aperture sonar using a single horizontal source beam (*S30*). This still required roughly an hour of surveying and so was subject to significant spatial and temporal aliasing of the shoal's dynamic morphology and population. Before this, fish groups at similar ranges were observed passing through a single horizontal source-receiver beam of a specially designed fixed sonar system over time (*S31-S33*).

Both OAWRS and CFFS rely on similar principles to estimate fish population density. The former requires well-established ocean-waveguide (*S2-S4, S11, S14, S34*) rather than free-space propagation (*S7, S18-S21*) modeling of the latter. OAWRS images of areal fish population density (Figs. 1A-B, 2A-D, 3A-D) are generated by compensating for (i) two-way transmission loss in the range-dependent continental-shelf waveguide through parabolic equation modeling, (ii) the spatially varying resolution footprint of the OAWRS system, (iii) fish target strength, and (iv) source power (*S2-S4*). The OAWRS areal

population densities are consistent with those obtained from conventional fish finding sonar (CFFS) over the same time period, as can be seen by comparing Figs. 2A-D with Fig. 2E, after integrating over depth in the roughly 10-m thick fish layer of the latter. This consistency is partly because both OAWRS and CFFS population density estimates depend on the expected scattering cross section of an individual fish, which we find to have a corresponding target strength of -45 dB *re* 1m in the 390-440Hz band of our experiment based upon tens of thousands of local measurements from the conventional sonar system. (This illustrates why the most effective uses of OAWRS technology in the near future will likely be in conjunction with CFFS and direct-capture measurements.) Our empirically measured target strength, however, is also consistent with a combination of theoretical modeling (*S3*) and empirical evidence gathered by National Marine Fisheries trawl samples obtained in the same location earlier in the same season as well as historically (*S35*). Catches in the area typically consist of a variable component of Atlantic herring, scup, hake, black sea bass, dogfish, and mackerel, all of which can have target strengths within an order of magnitude of each other in the 390-440 Hz range, which is near or just below swim-bladder resonance for many of these species (*S36*).

To generate the spatial power spectrum shown in Fig. 1C, the 2-D Fourier transform of an instantaneous OAWRS areal fish density image was computed. Squared magnitudes of 2-D transforms of 10 consecutive OAWRS images, over an 8 minute period, were combined by standard periodigram averaging to obtain an estimate of the 2-D spectrum of areal population density. This estimated spectrum corresponds to the Fourier transform of the 2-D autocorrelation function of areal fish population density, normalized so that the correlation at zero-spatial lag, which is the integral of the 2-D spectrum, is the second statistical moment of areal population density. Apart from expected asymmetries arising from variations in the range and cross-range resolution of our imaging system, the resulting 2-D spectra showed uniform azimuthal dependence in wavenumber which was repeatable throughout all our observations of the shoals and scattered fish groups regardless of their orientation with respect to our measurement system. The radial-wavenumber dependence of the spectrum was then estimated by averaging within a roughly 20^{o} azimuthal wavenumber spread where the resolution of our imaging system is highest. Two periods were chosen, one at 16:19 EST of May 14 with a very large shoal present and the other at 21:30 EST of May 9 with only small scattered groups present. The 2-D spectrum was then multiplied by radial wavenumber, which is the Jacobian of the coordinate transform from Cartesian to polar, and normalized so that the 1-D integral over spatial frequency, or radial wavenumber, of either curve plotted in Fig. 1C yields the mean of the square of areal fish density over the survey area. The power laws shown in Fig. 1C were obtained by least squares fits. These results are very stable. They were repeated 4 times at uniform intervals: on May 14 from 9:34 EST to 17:02 EST, leading a mean power law of -1.55 with a 0.04 standard deviation, and on May 9, from 17:10 EST to 17:50 EST leading to a mean power law of -1.46 with a 0.03 standard deviation.

Transmission scintillation from randomness in the ocean medium due to such effects as internal waves and turbulence, and fluctuations in the received field due to source-receiver motion, and scattering from fish schools and ocean boundaries, ultimately introduce relatively little uncertainty in OAWRS images, since a standard deviation of roughly 1-dB per pixel (*S11*) is expected after our intensity averaging of the expected CCGRF measurements. (A standard deviation of less than 1-dB per pixel corresponds to

an error of less than 25% in any OAWRS intensity or areal population density estimate for the given pixel.) We applied a temporal running average window of 5-consecutive OAWRS images (250 seconds) and averaged over 2 adjacent 15-m range resolution cells to produce each image presented in Figs. 1A-B, 2A-D, 3A-D, and time series in Figs. 3E-G.

Contributions from millions of fish over hundreds of independent pixels were summed to form the population estimates of Fig. 3E. Our calculations show that fluctuations from propagation scintillation or variations in fish scattering cross-section should then lead to errors of less than 1% of the estimated value for any given temporal population sample, given the law of large numbers (*S37*).

The coherence area of Fig. 3G is the area within one e-folding length of the 2-D fish density autocorrelation function within a shoal. The coherence area is a quantitative way of describing the extent of concentrated population centers within a shoal. It is the area within which population density should not vary significantly. The decrease in coherence area in proportion with the decrease in shoal area and fish population, Fig. 3, is consistent with fish assembly and reassembly models (*S38-S40*).

The location of a population center (Figs. 3A-D) is here defined as the centroid of a local coherence area containing a population density maximum. Estimation of such a centroid involves averaging areal fish population density over a coherence area that includes roughly 30 independent range pixels. This, multiplied by the 10 independent samples from the time and range averaging used to generate each pixel, described previously, leads to μ = 300 independent samples, which reduces the speckle-noise standard deviation in fish population density to roughly $4.34/\sqrt{\mu}$ = 0.25 dB (*S10, S11*) corresponding to less than a 6% uncertainty in mean areal fish density over the coherence area. The same standard deviation and percent error is found in the mean of an equal annular area surrounding the coherence area. The image contrast, or difference in dB between the mean fish density within the coherence area and that of an equal area surrounding it, is approximately 5 dB, which is more than an order of magnitude higher than the 0.25 dB standard deviation from speckle noise. This ensures that the effect of speckle noise on our calculations of motions of mass centers is negligible. The observed horizontal separation rate, or divergence rate, of the two population centers (Fig. 3H) is consistent with the observed variations in total population (Fig. 3E), and the lower limits of OAWRS sensitivity to fish returns before seafloor scattering mechanisms become important (*S2-S4, S11, S14*).

Before adopting the fish density wave explanation, we investigated other possible causes of relative motion between population centers, all of which had to be ruled out. Effects related to the motion of our OAWRS research vessel and ocean internal waves were dismissed because these are one order of magnitude slower than the relative motions we observed between population centers. Surface gravity waves are also much slower, incoherent, and of much smaller amplitude at the time than the acoustic wavelength. We also investigated possible artifacts that could be caused by sidelobe leakage and beam merging of fish groups. We found these to be two orders of magnitude lower in speed than the observed density waves. Finally, noise from passing ships appearing as beams in OAWRS images had levels orders of magnitude lower than scattered returns from the

tracked population centers, so this mechanism was also ruled out. Most peaks shown in Fig. 3H contain multiple points leading to the apex, consistent with the coherent motion of a wave at the speeds indicated.

Fish density waves have been previously observed to propagate over meter scales, reaching maximum speeds of up to 15 m/s, in tank experiments. (*S41-S43*). These density waves could be a mechanism to signal group behavioral change similar to that described by "synchrokinesis" (*S39, S44*).

No correlation was found between OAWRS imagery and sub-bottom geologic features, after extensive investigation (*S4*).

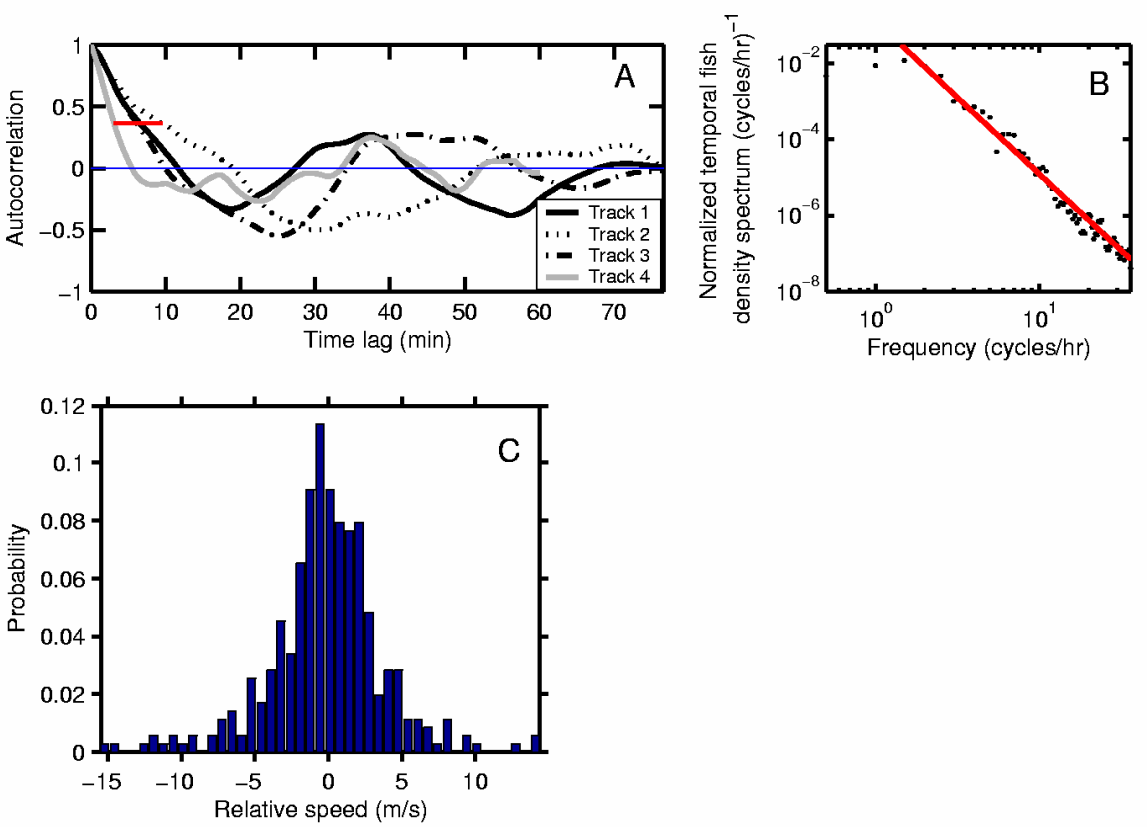

Fig. S1. (**A**) Autocorrelation functions, with red horizontal line indicating e-folding times, and (**B**) frequency power spectrum, with frequency to the -2 dependence, for the shoal population time series (blue curve in Fig. 3E). No remarkable periodicity is found. (**C**) Histogram of all relative speeds measured in Fig. 3H.

Supporting References and Notes

S1. C. B. Officer, *Introduction to the Theory of Sound Transmission* (McGraw-Hill, New York, 1958).

S2. N. C. Makris, L. Avelino, R. Menis, *J. Acoust. Soc. Am*. **97**, 3547 (1995).

S3. P. Ratilal, thesis, Massachusetts Institute of Technology (2002).

S4. P. Ratilal *et al*., *J. Acoust. Soc. Am*. **117**, 1977 (2005).

S5. C.-S. Chia *et al*., *J. Acoust. Soc. Am*. **108**, 2053 (2000).

S6. L. M. Brekhovskikh, Y. P. Lysanov, *Fundamentals of Ocean Acoustics* (Springer, New York, ed. 3, 2003).

S7. H. Medwin, C. Clay, *Fundamentals of Acoustical Oceanography* (Academic Press, Boston, 1998).

S8. W. Siebert, *Circuits, Signals, and Systems* (MIT Press, Cambridge, 1986), pp. 435-439.

S9. J. W. Goodman, *Statistical Optics* (Wiley, New York, 1985).

S10. N. C. Makris, *Opt. Lett.* **20**, 2012 (1995).

S11. N. C. Makris, *J. Acoust. Soc. Am*. **100**, 769 (1996).

S12. S. M. Kay, *Fundamentals of Statistical Signal Processing: Estimation Theory* (Prentice-Hall, Upper Saddle River, 1993), vol. 1.

S13. N. C. Makris, *J. Acoust. Soc. Am.* **106**, 2491 (1999).

S14. N. C. Makris, P. Ratilal, *J. Acoust. Soc. Am*. **109**, 909 (2001).

S15. I. Dyer, *J. Acoust. Soc. Am*. **48**, 337 (1970).

S16. Ratilal, Makris, *J. Acoust. Soc. Am.* **118**, 3532 (2005).

S17. Chen, Ratilal, Makris, *J. Acoust. Soc. Am.* **118**, 3560 (2005).

S18. O. Sund, *Nature* **135**, 953 (1935).

S19. R. Balls, *Journal du Consiel Permanent International Pour L'exploration de la Mer*. **15**, 193 (1948).

S20. O. A. Misund, *Fish Biology and Fisheries* **7**, 1 (1997).

S21. D. N. MacLennan, E. J. Simmonds, *Fisheries Acoustics* (Chapman & Hall, London, ed. 2, 1992).

S22. F. Gerlotto, M. Soria, P. Fréon, *Can. J. Fish. Aquat. Sci*. **56**, 6 (1999).

S23. H.-S. Niwa, *J. Theor. Biol*. **235**, 419 (2005).

S24. O. A. Misund, A. Fernö, T. J. Pitcher, B. Totland, *ICES J. Mar. Sci.* **55**, 58 (1998).

S25. T. J. Pitcher, O. A. Misund, A. Fernö, B. Totland, V. Melle, *ICES J. Mar. Sci.*, **53**, 449 (1996).

S26. M. T. Hafssteinson, O. A. Misund, *ICES J. Mar. Sci.*, **52**, 915 (1995).

S27. L. Nøttestad, A. Fernö, S. Mackinson, T. J. Pitcher, O. A. Misund, *ICES J. Mar. Sci.*, **59**, 393 (2002).

S28. A. Fernö *et al.*, *Sarsia* **83**, 149 (1998).

S29. F. Gerlotto, J. Paramo. *Aquat. Living Resour.* **16**, 113 (2003).

S30. J. S. M. Rusby, M. L. Somers, J. Revie, B. S. McCartney, A. R. Stubbs, *Marine Bio.* **22**, 271 (1973).

S31. D.E. Weston, J. Revie, *J. Sound Vib.*, **17**, 105 (1971).

S32. J. Revie, G. Wearden, P. D. Hocking, D. E. Weston*, J. Const. Int. Explor. Mer*. **36**, 82 (1974).

S33. D. E. Weston, H. W. Andrews, *J. Acoust. Soc. Am.* **87**, 673 (1990).

S34. N. C. Makris, *J. Acoust. Soc. Am*. **94,** 983 (1993).

S35. http://www.nmfs.noaa.gov/

S36. R. W. Nero, C. H. Thompson, J. M. Jech, *ICES J. Mar. Sci.* **61**, 323 (2004).

S37. A. W. Drake, *Fundamentals of Applied Probability Theory*, (McGraw-Hill, New York, 1967), pp. 203-216.

S38. T. J. Pitcher, *Scientia Marina*, **59**, 295 (1995).

S39. T. J. Pitcher, in *Encyclopedia of Ocean Sciences*, J. H Steele, K. K. Turekian, S. A. Thorpe, Eds. (Academic Press, London, 2001), pp. 978-987

S40. T. J. Pitcher, in *Developing and Sustaining World Fisheries Resources: The State of Science and Management, Proceedings of the 2nd World Fisheries Congress*, D. A. Hancock, D. C. Smith, A. Grant, and J. P. Beumer, Eds. (CSIRO, Collingwood, 1997), pp. 143-148.

S41. C. M. Breder, *Bull. Am. Mus. Nat. Hist.* **117**, 399 (1959)

S42. D. V. Radakov, in *Schooling in the Ecology of Fish*, D.V. Radakov, Eds. (Wiley, New York, 1973), pp.77-99.

S43. E. Shaw, in *Development and Evolution of Behavior*, L. R. Aronson, E.Tobach, D. S. Lehrman, J. S. Rosenblatt, Eds. (Freeman, San Francisco, 1970), pp. 452-480.

S44. U. Kils, thesis, Christian-Albrechts-Universität zu Kiel (1986).